Published version of this article can be found at: http://dx.doi.org/10.1016/j.physb.2012.01.094

An X- and Q-band Gd^{3+} EPR study of a single crystal of $EuAlO_3$: EPR linewidth variation with temperature and low-symmetry effects

Sergey I. Andronenko,[1] Roza R. Andronenko,[2] Sushil K. Misra[3]

[1] Physics Department, Kazan Federal University, Kremlevskaya 18, Kazan, 420008, Russia

[2] Institute of Silicate Chemistry, nab. Makarova 2, St-Petersburg, 199034, Russia

[3] Physics Department, Concordia University, 1455 de Maisonneuve Boulevard West, Montreal, Quebec H3G 1M8, Canada.

e-mail: skmisra@alcor.concordia.ca

Detailed electron paramagnetic resonance (EPR) studies on a single crystal of Gd^{3+}-doped Van Vleck compound $EuAlO_3$, potentially a phosphorescent/ luminescent/laser material, with the Gd^{3+} ion substituting for the Eu^{3+} ion, were carried out at X-band (9.2 GHz) over the 77 – 400 K temperature range. They provide new physical results on magnetic properties of the Eu^{3+} ion in a low symmetry environment. The asymmetry exhibited by the variation of the Gd^{3+} EPR line positions for the orientations of the external magnetic field about the Z and X magnetic axes in the ZX plane was ascribed to the existence of low, monoclinic, site symmetry, as revealed by the significant values of the spin-Hamiltonian (SH) parameters b_4^1, b_4^3, estimated by fitting all the observed EPR line positions at room temperature for the orientation of the magnetic field in the magnetic ZX plane using a least-square fitting procedure. The temperature dependence of the Gd^{3+} EPR linewidth is interpreted to be due to the "life-time" broadening, caused by dynamical exchange and dipolar interactions between the impurity Gd^{3+} ions and the host Eu^{3+} ions.

P.A.C.S. Classification: 76.30 Kg

I. Introduction

$RAlO_3$ (R = rare earth) single crystals, characterized by the perovskite structure at and below room temperature, are interesting due to their phosphorescence and luminescence properties [1,2] as well as for their use as laser materials [1]. There exists further interest in perovskite-like compounds because of possessing a structure similar to that of manganites, which exhibit giant magnetostriction. Its peculiarities can be investigated in mixed compounds, where Al ions are partly replaced by Mn [3,4] ions. A detailed electron paramagnetic resonance (EPR) investigation of the Gd^{3+} ion in the isostructural crystal $LaGaO_3$ was recently reported by Vazhenin et al. [5]. Low symmetry effects in Gd^{3+} and Fe^{3+} spectra in $YAlO_3$ were also analyzed with the use of maximum invariant components (MIC) in [6]. Physical properties of $EuAlO_3$ have not yet been investigated extensively. A preliminary investigation of Gd^{3+} EPR spectra in an $EuAlO_3$ single crystal was carried out by Andronenko et al. [7]. In addition, EPR studies on the Cr^{3+} ion in $EuAlO_3$ have been reported [8], as well as those on Gd^{3+} in the isostructural $LaAlO_3$ and $YAlO_3$ crystals [9,10]. A relevant detailed EPR study of the Gd^{3+} ion in monoclinic $La_2Si_2O_7$ and $LaNbO_4$ crystals, which are also characterized by a low (C_S, and C_2, correspondindly) point symmetry of the Gd^{3+} ion and exhibit low-symmetry effects, was reported by Misra and Andronenko [11,12].

Europium aluminate ($EuAlO_3$) is an insulating Van-Vleck paramagnet, whose paramagnetism is due to the admixture of the levels of the $^7F_1$ term, split by the orthorhombic crystal field into three singlets (281, 359, and 479 cm^{-1}), in the singlet ground state $^7F_0$ [13], which by itself is non-magnetic. This admixture makes it paramagnetic, known as Van-Vleck paramagnetism. For a review of the peculiarities of magnetic resonance in Van-Vleck paramagnets, see Aminov et al.[14].

This paper reports a detailed EPR investigation on the Gd^{3+} ion in $EuAlO_3$ single crystal at X-band (9.22 GHz). The EPR spectra are recorded for various orientations of the external magnetic field (**B**) in the magnetic ZX plane in the 77 – 400 K range. [The magnetic Z, X, Y axes are defined to be those orientations of **B** for which the extrema of the allowed line positions ($\Delta M = \pm 1$; M is the electronic magnetic quantum number) occur; of these the maximum splitting of the EPR lines occurs for **B** along the magnetic Z-axis, while the minimum splitting of EPR lines occurs for **B** along the magnetic Y axis]. Some additional measurements were made at Q-band (36 GHz) at 140 K.

The EPR data enable one to: (i) determine the local symmetry at the site of the Gd^{3+} ion; (ii) estimate accurately the values of all the Gd^{3+} spin-Hamiltonian (SH) parameters in the $EuAlO_3$ single crystal at 77 and 295 K; and (iii) analyze the EPR line broadening due to the dynamical magnetic interactions of the Eu^{3+} host ions with the Gd^{3+} impurity ions.

II. Crystal structure and sample preparation

Single crystals of $EuAlO_3$ were grown by crystallization from a molten solution; they were parallelepipeds of ~ 2×2×3 mm dimensions. At room temperature, single crystals of $EuAlO_3$ are characterized by the orthorhombic space-group symmetry D_{4h}^{16}. There exists C_S point symmetry at the Eu^{3+} sites, substituted for by the Gd^{3+} ions. The reflection plane is normal to the c crystallographic axis, which can be considered as a pseudo two-fold axis. The lattice parameters of $EuAlO_3$ are: a = 5.271 Å, b = 5.292 Å, c = 7.458 Å, the distance between two adjacent Eu^{3+} ions being 3.732 Å, as determined by Geller and Bala [15]. Further refinement of the orthorhombic aluminate structure was carried out by Marezio et al [16]. The unit cell of $EuAlO_3$ crystal contains four Eu^{3+} ions, located at two sets of magnetically inequivalent sites [17]. Thus, two distinct sets of Gd^{3+} EPR spectra are expected. These sets are reflections of each other in the planes perpendicular to the a and b axes. As a consequence, the Y-axes of these magnetically inequivalent Gd^{3+} ions are coincident, oriented along the c-axis, whereas the Z and X axes lie in the ab plane. A single crystal of $EuAlO_3$ possesses the shape of a thin rectangular plate, with the c-axis being oriented along the larger dimension of the plate. The (001), (010), and (100) faces of the crystal are pseudocubic.

Synthesis. The $EuAlO_3$ compound was first synthesized in powder form following the standard solid-phase reaction by mixing high-purity (99.9%) Eu_2O_3 and Al_2O_3 compounds in stoichiometric proportions and maintaining the mixture at 1600° C, which contain trace amounts of Gd^{3+} as impurities. The completion of the reaction was verified by X-ray diffraction and chemical analysis. The crystals were then grown from the melt of this powder in Ar atmosphere. The single crystals may exhibit twinning with the following twinning pattern: the c axes are coincident, whereas the a and b axes are transposed. However, no twinning was found in the investigated crystals.

III. Experimental results

The spectra were recorded at 77 K, as well as in the range 120 to 400 K at X-band frequencies 9.05 and 9.22 GHz, respectively; some additional measurements were made also at Q-band (36 GHz) at 140 K. The X-band EPR spectra of Gd^{3+}: $EuAlO_3$ were recorded on a RE1306 spectrometer, equipped with a liquid-nitrogen gas-flow temperature controller (120 - 400 K). Two sets of EPR lines from Gd^{3+} ions at magnetically inequivalent sites were observed. The room-temperature (RT, 295 K) and liquid-nitrogen temperature (77 K) Gd^{3+} EPR spectra are shown in Figs. 1(a) and 1(b) for the orientation of the magnetic field (**B)** along the magnetic Z-axis of one of the magnetically inequivalent Gd^{3+} ions; the allowed transitions $M \leftrightarrow M + 1$ for the second magnetically inequivalent Gd^{3+} ion are indicated by Z′. Figure 1 (c) shows Gd^{3+} EPR spectrum for **B** || Y, Y′-axes, which are both parallel to the crystallographic c-axis. The Q-band (36 GHz) EPR spectrum is shown in Fig. 1(d) at 140 K for B | | Z-axis. From Figs. 1(a) – 1(d), it is seen that additional EPR lines are observed, whose magnetic axes are not coincident with any crystallographic plane of the crystal. They are most likely due to Eu^{2+} ion present as impurity. No further analysis is made here of these lines due to their large linewidth and complexity.

Figure 2 shows the RT angular variation of Gd^{3+} EPR line positions in $EuAlO_3$ for the orientations of **B** in the magnetic ZX plane. The angle between the b-axis and the magnetic Z-axes for the two magnetically inequivalent Gd^{3+} sites in the ab plane are $\alpha = \pm(13 \pm 1)°$ in $EuAlO_3$ as seen from Fig. 2; these do not change with temperature. The value of α for Gd^{3+} is very close to 16º for Gd^{3+}: $LaGaO_3$ [5], and it differs considerably from those for Er^{3+} ($\alpha = 38°$) and Yb^{3+} ($\alpha = 30°$) in $EuAlO_3$ [18, 19].

The angular variation of the line positions for the orientations of **B** in the ZY magnetic plane was found to be symmetrical about the Z and Y axes, unlike that in the ZX plane which is not symmetrical about the Z and X axes. It is seen from Fig. 2, showing the angular variation of line positions for the orientation of **B** in the ZX plane that the extrema of the line positions for **B** about the X-axis for the various EPR transitions are non-coincident and non-symmetrical about the magnetic Z and X axes. This indicates monoclinic symmetry at the Gd^{3+} sites.

IV. Spin-Hamiltonian parameters

The asymmetry of line positions about the Z- and X-axes in the angular variation of Gd^{3+} EPR line positions in the ZX plane reveals existence of a monoclinic symmetry at the Gd^{3+} sites. The low-symmetry effects for C_S point symmetry were discussed in [20, 21], pointing out the

similarity of C_2 (real two-fold axis) and C_S (pseudo two-fold axis). Therefore, the observed EPR spectra are described by the following SH, as discussed by Misra and Rudowicz [22] and by Misra [21] for C_S | | Y-axis,

$$\mathcal{H} = \mu_B[g_z S_z B_z + g_x S_x B_x + g_y S_y B_y + g_{xz}(S_x B_z + S_z B_x)]$$

$$+ \sum_{m=0,1,2} (1/3) b_2^m O_2^m + \sum_{m=0,1,2,3,4} (1/60) b_4^m O_4^m + \sum_{m=0,1,2,3,4,5,6} (1/1260) b_6^m O_6^m \qquad (1)$$

In Eq. (1), μ_B is the Bohr magneton; g_z, g_x g_y are the diagonal elements of the g-matrix, and g_{xz} is the only nonzero off-diagonal element of the g-matrix, **S** (S=7/2) is the electron spin operator for the Gd^{3+} ion; b_n^m are the ZFS parameters; and the O_n^m are the operator equivalents as defined by Abragam and Bleaney [23], whose matrix elements are listed by Misra [21] including those with negative m, which were not included in Abragam and Bleaney [23].The notion of extended Stevens operators, i.e. full set of operator equivalents O_n^m, was first introduced in [24]; for a review of other operators used in EMR, see, [21, 25, 26].

Three different orientations of the axes, with their symmetry axes (C_S, C_2) being parallel to the X, Y, Z magnetic axes, respectively, lead to three different spin Hamiltonians. The corresponding non-zero SH parameters were discussed in [22, 29], and later used for the interpretation of low-symmetry effects in [30]. In the present case of $EuAlO_3$, the Y-axis has been chosen to be that direction of the magnetic field for which the extrema of the line positions occur for the same direction of the magnetic field. The Z, X-axes are then in the plane perpendicular to it, which is the ab plane. Further, the Z-axis has been chosen to be such that $b_2^2 / b_2^0 \leq 1$. Thus, the other two extrema of the line positions, which are slightly non-coincident, lie very close to the principal Z- and X-axes of the D-tensor, as discussed in [30]. The C_S-axis in $EuAlO_3$ has here been chosen to be parallel to the Y-axis, so that only those b_n^m, where m (≤ n) are odd and positive and n are 2, 4, 6, describe the low-symmetry observed in the ZX plane. The same orientations of the axes was used in [6] for the interpretation of low-symmetry for Gd^{3+} in $LaGaO_3$ crystal, which is isostructural to $EuAlO_3$. Alternatively, for Gd^{3+} in $La_2Si_2O_7$ [11], the C_S-axis is parallel to the X-axis, so that only those b_n^m, where m (≤ n) are odd and negative and n are 2, 4, 6, are non-zero. This is also the case for Gd^{3+} in $LaNbO_4$ and $PrNbO_4$ [12]. The third

case, where C_S is parallel to the Z-axis, occurs for Gd^{3+} in $YAlO_3$ [6], where only those b_n^m, where m ($\leq$ n) are even and negative and n are 2, 4, 6, describe the low-symmetry.

The values of the SH parameters at liquid-nitrogen and room-temperature, listed in Table 1, were estimated by fitting simultaneously all X-band EPR line positions (142 and 323, respectively, in total) observed for the various orientations of **B** in the ZX plane by the least-squares (LSF) fitting technique using the eigenvalues and eigenvectors of the SH matrix [27]. The estimation of b_2^0 and b_2^2 parameters was obtained from the Q-band Gd^{3+} EPR line positions observed about the Z- and X-axes. The energy levels of the Gd^{3+} ion for these parameters are shown in Fig. 3, wherein the corresponding allowed X- and Q-band transitions are also indicated. An inspection of Table 1 reveals the following: the low-symmetry exhibited is confirmed by the significantly large values of the SH parameters g_{xz}, b_2^1, b_4^1, b_4^3. The sign of b_2^0 is assumed to be negative, in accordance with the sign of b_2^0 in others perovskites [5], in the absence of liquid-helium temperature data, which are required to determine this sign unequivocally. The signs of the other parameters b_n^m relative to b_2^0 are determined correctly by the LSF procedure. The parameters b_6^k could not be estimated precisely at 77 and 295 K from the experimental line positions, due to their being too small. The second set of Gd^{3+} EPR lines can be satisfactorily described by the same values and signs of all the SH parameters, except for the signs of the parameters b_2^1, b_4^1, b_4^3 being opposite. These values are consistent with those reported in [7] after appropriate transformation of the magnetic axes (b_2^0 = -1.92) to relate to the present case [28].

The g_z, g_x, g_y values for Gd^{3+} deviate somewhat from 1.992, which is the typical g-value for the Gd^{3+} ion. In particular, this deviation is negative for g_z. These deviations are due to the admixture of the higher excited levels $^6P_{7/2}$ and $^6D_{7/2}$ of Eu^{3+} in the ground state [31]. Gd^{3+} is an S-state ion, therefore the crystal field acts only very weakly, causing only slight deviations of the three g-values, similar to that for $EuVO_4$ [32] and $PrVO_4$ [33].

V. Temperature dependence of Gd^{3+} EPR linewidth. The linewidth behavior in the 77 – 400 K temperature range is shown in Fig. 4. It is first noted that the imperfections and defects in the crystal cause the outer EPR lines to become broader than the central one, independent of

temperature [23]. There is observed an increase in the EPR linewidth with increasing temperature. This is accounted for in the same way as that for the Van-Vleck paramagnet crystal $PrNbO_4$ [12]. Specifically, it is due to the dynamical exchange and dipolar interactions between Gd^{3+} and the host paramagnetic Eu^{3+} ions, which cause a significant temperature dependence of the linewidth, described as follows. When the excited states of the Eu^{3+} ion, lying at 281, 359 and 479 cm^{-1} above the singlet ground state $^7F_0$ begin to become more and more populated as the temperature increases, the Gd^{3+} EPR linewidth starts to increase due to enhanced Gd^{3+}-Eu^{3+} interactions. The fluctuating dipolar and exchange fields produced by the host Eu^{3+} ions at the sites of the impurity Gd^{3+} ions cause "lifetime broadening" [32,33,34], caused by the fluctuating components of the magnetic fields perpendicular to the external field at the Gd^{3+} ion. This was referred to as "nonsecular broadening" by Kubo and Tomita [35]. The low-frequency components of the fluctuating fields parallel to the external field are expected to have rather small amplitudes, causing a negligible "secular" (longitudinal) broadening. On the other hand, the "lifetime broadenings" due to dynamic dipolar and exchange fields, as exhibited by the allowed transitions $\Delta M = \pm 1$, are significant and proportional to the transition probabilities $\left|\langle M \pm 1|S_{\pm}|M\rangle\right|^2$. The "lifetime broadening" of the M level by the dynamic dipolar and exchange fields is expressed as a sum of two contributions [34]:

$$\Delta B(M) = \Delta B_{+} + \Delta B_{-} = a(\left|\langle M+1|S_{+}|M\rangle\right|^2 + \left|\langle M-1|S_{-}|M\rangle\right|^2 \qquad (2)$$

The width of the line corresponding to the transition $M \leftrightarrow M-1$ is then calculated to be:

$$\Delta B(M \leftrightarrow M-1) = \Delta B(M) + \Delta B(M-1) = b[2S(S+1)-2M(M-1)-1] , \qquad (3)$$

In Eqs. (2) and (3), a and b are temperature-dependent proportionality coefficients.

The ratios of the EPR linewidths for the various allowed transitions, $\Delta B(M \leftrightarrow M\pm1)$ at 295 K, calculated using Eq. (3), are listed in Table 2 which also includes the corresponding ratios of the experimentally observed lines. These two ratios are in reasonably good agreement with each other, thus confirming the influence of "lifetime broadening". In calculating these ratios, the temperature-independent EPR linewidths, specifically those at 77 K (Fig. 4), was subtracted off from the observed EPR linewidths. As for the temperature dependence of the linewidth contained in the coefficient b in Eq. (3), it can be accounted for by the theory of temperature dependence of EPR linewidth in magnetic compounds, where the magnetic ion has

even numbers of unpaired electrons as in Van-Vleck paramagnets, as developed by Sugawara and Huang [36]. Accordingly, the EPR linewidth expressed as:

$$\Delta B_{pp} \propto kT\cdot(\chi_T - \chi_{iso}) \qquad (4)$$

where χ_T is isothermal susceptibility, and χ_{iso} is the isolated susceptibility.

As for the susceptibility, according to Holmes *et al*. [13], the magnetic susceptibility of $EuAlO_3$ along the Y-axis is determined by the matrix elements between the wave functions of the ground-state singlet, F_0, and the central excited singlet of the manifold $^7F_1$ (359 cm^{-1}). The magnetic susceptibility along the Z-axis is determined by the matrix element between the wave functions of the same ground-state singlet and the lowest excited singlet of the manifold $^7F_1$ (281 cm^{-1}), whereas the magnetic susceptibility along the X-axis is determined by the matrix elements between the wave functions of the ground-state singlet and the highest excited-state singlet of the manifold $^7F_1$ (479 cm^{-1}).

The temperature dependence of the EPR linewidth of the impurity ions in Van-Vleck paramagnets with singlet ground state is then expressed as [36]:

$$\Delta B_{pp} = \Delta B_{dia} + A\cdot \sum_{i=x,y,z} \left\langle \phi_{ground} \left| J_i \right| \phi_{excited} \right\rangle^2 \cdot \exp(-\Delta_{excited} / kT) /Z, \qquad (5)$$

where, ΔB_{dia} is the EPR linewidth in diamagnets (temperature independent); φ_{ground} is wave function of the ground-state singlet; $\varphi_{excited}$ is the wave function of the excited state; $\Delta_{excited}$ is the energy of the excited state; *i* stands for x, y, z; Z is the partition function; and A is the dimension parameter.

For illustration, the EPR linewidth of for B || X-axis for the Gd^{3+} ion is analyzed here. The linewidth of the Gd^{3+} ion for B || X-axis depends on the dipolar and exchange fields induced by the magnetic moments of Eu^{3+} ions for this direction of the magnetic field. The total magnetization of orthoaluminate was analyzed in [37] as a sum of two magnetic sublattices, assuming low-symmetry crystal field (C_S) at the rare-earth ion sites. Using this approach, and exploiting Eq. (5), it can be shown that the temperature dependence of the EPR linewidth can be expressed by the following expression:

$$\Delta B_{pp} = \Delta B_{dia} + (C_1\cdot exp(-\Delta_3 / kT)+C_2\cdot exp(-\Delta_1/kT)) /Z, \qquad (6)$$

where ΔB_{dia} is the temperature-independent EPR linewidth, which can be assumed to be that at 77 K, at which the energy levels of the manifold $^7F_1$ are not populated, Z =

$1+exp(-\Delta_1/kT)+exp(-\Delta_2/kT)+exp(-\Delta_3/kT)$, Δ_1 = 281, Δ_2 = 359, Δ_3 = 479 cm^{-1}. The constants $C_1 = A\langle\varphi_0|J_x|\varphi_3\rangle^2$ and $C_2 = A\langle\varphi_0|J_y|\varphi_1\rangle^2$ in Eq. (6) are used as fitting parameters. The best-fitted values are: C_1 = (363 ± 5) G and C_2 = (0 ± 5) G. The fitted temperature dependence the Gd^{3+} transition 1/2↔3/2 is shown in Fig. 4.

VI. Concluding remarks

The salient features of the EPR study of the Gd^{3+} ion in $EuAlO_3$ crystal presented in this paper are as follows:

(i) The SH parameters for the Gd^{3+} ion situated at a Eu^{3+} site have been estimated accurately at 77 and 295 K. Two sets of magnetically inequivalent Gd^{3+} ions were found from the EPR spectra, consistent with the symmetry of the host Eu^{3+} ions. Additional set of EPR lines was observed, most likely from Eu^{2+} ions.

(ii) The relative values of the EPR linewidths for different Gd^{3+} EPR transitions have been interpreted to be due to the "life-time" broadening.

(iii) Theoretical considerations of Sugawara and Huang [36] have been successfully applied to explain the linewidth broadening of the impurity ion Gd^{3+} in the Van-Vleck paramagnet $EuAlO_3$.

It is hoped that the results presented here will be also useful in the studies of the $EuAlO_3$ compound as a suitable phosphorescent/laser material.

Acknowledgements. S.K.M. is grateful to the Natural Sciences and Engineering Research Council of Canada for partial financial support and S.I.A. is grateful to Ministry of Education of Russian Federation for partial support in the framework of the program "Development of scientific potential of higher school".

References

[1] A.A. Kaminskii, Laser crystals: their physics and properties, Springer-Verlag, New York, 1990.

[2] K. I. Portnoi and N. I. Timofeeva, Kislorodnue Soedinenia R.Z.E., Metallurgia, Moscow, 1986.

[3] S.I. Andronenko, R.R. Andronenko, O.A. Zagrebel'nyi, N.V. Chezhina, Glass Phys. Chem. 35 (2009) 652 –659.

[4] S.I. Andronenko, R.R. Andronenko, O.A. Zagrebel'nyi, Glass Phys. Chem. 36 (2010) 617-622.

[5] V.A. Vazhenin, A.P. Potapov, V.B. Guseva and M.Yu. Artyomov, Phys. Solid State 5 (2009) 917-923.

[6] N.M. Nizamutdinov, N.M. Khasanova, A.A. Galeev, G.R. Bulka, V.M. Vinokurov, V.A. Akkerman, G.A. Ermakov, Sov. Phys. Crystallography 34 (1989) 536-541.

[7] S.I. Andronenko, L.N. Koroleva, I.A. Bondar', and V.A. Ioffe, Sov. Phys. Solid State 24 (1982) 881 – 882.

[8] J.P. Van der Ziel, F.R Meritt, L.G. Van Uitert, J. Chem. Phys. 50 (1969) 4317-4319.

[9] W. Low, A. Zusman, Phys. Rev. 130 (1963) 144-150.

[10] R.L. White, G.F. Herrmann, J. W. Carson, M. Mandel, Phys. Rev. A136 (1964) 231-239.

[11] S. K. Misra and S. I. Andronenko, Appl. Magn. Res. 32 (2007) 377-384.

[12] S.K. Misra, S.I. Andronenko, and T. Yu. Chemekova, Phys. Rev. B 67 (2003) 214411 (1-7).

[13] L. Holmes, R. Sherwood, L.G. Van Uitert, S. Hüfner, Phys. Rev. 178 (1969) 576-579.

[14] L.K. Aminov, B.Z. Malkin, M.A. Teplov, in K.A. Gschneidner, Jr and L. Eyring (Eds.), Handbook on the Physics and Chemistry of Rare Earths, v. 22, Elsevier B.V.,1996, pp. 295-506.

[15] S. Geller, V.B. Bala, Acta Cryst. 9 (1956) 1019-1025.

[16] M. Marezio, P.D. Dernier, J.P. Remeika, J. Sol. St. Chem. 4 (1972) 11-19.

[17] M.L. Meilman and M.I. Samoilovich, Introduction in EPR spectroscopy of activated single crystals, Atomizdat, Moscow, 1977.

[18] P. Bonville, J.A. Hodges, P. Imbert, J. Phys. 41 (1980) 1213-1223.
[19] P. Bonville, J. A. Hodges, P. Imbert, F. Hartmann-Boutron, Phys. Rev. B18 (1978) 2196-2208.
[20] J.R.Pilbrow and M.R. Lowrey, Rep. Prog. Phys., 43(1980), 433-496.
[19-21] S. K. Misra, Multifrequency Electron Paramagnetic resonance: Theory and Applications, Wiley-VCH, Weinheim, Germany (2011), Chapter 7, and Table 7.2.
[22] S.K. Misra and C. Rudowicz, phys. stat. sol. (b) 147 (1988) 677-684.
[231] A. Abragam and B. Bleaney, Electron Paramagnetic resonance of Transition Ions, Clarendon, Oxford (1970).
[24] C. Rudowicz, J. Phys. C18 (1985) 1415-1430; corrigendum J. Phys. C19 (1985) 3837.
[25] C. Rudowicz, Magn. Res. Rev. 13 (1987) 1-89; ibidem 13 (1988) 335.
[26] C. Rudowicz and S.K. Misra, Applied Spectroscopy Reviews, 36 (2001) 11-36.

[27] S.K. Misra, J. Magn. Res. 23 (1976) 403-410.
[28] D. A. Jones, J. M. Baker, and D. F. D. Pope, Proc. Phys. Soc. 74 (1959) 249-256.
[29] C. Rudowicz, J. Chem. Phys. 84 (1986) 5045-5058.
[30] T.H. Yeom, C. Rudowicz, S.H. Choh, D.G. McGavin, phys. stat. sol. (b), 198 (1996) 839.
[31] D. J. Newman, W. Urban, J. Phys. C: J. Sol. St. Phys. 5 (1972) 3101-3109.
[32] F. Mehran, K.W. Stevens, T.S. Plaskett, Phys. Rev. B22(1979)1817-1823.
[33] S.I. Andronenko, V.A. Ioffe, Yu. P. Udalov, 1981, Sov. Phys. Solid. State. 23 (1981) 1478-1479.
[34] F. Mehran, K.W. Stevens, T.S. Plaskett, W. J. Fitzpatrick, Phys. Rev. B22 (1980) 2206-2212.
[35] R. Kubo and K. Tomita, J. Phys. Soc. Jpn. 9 (154) 888-919.
[36] K. Sugawara and C.Y. Huang, 1976, J. Phys. Soc. Jpn. 41 (1976) 1534-1539.
[37] S.I. Andronenko, A.N. Bazhan., L.P. Mezentseva, Sov. Phys. Solid. State. 32 (1990) 455-457.

Table 1. The spin-Hamiltonian parameters of the Gd^{3+} ion in $EuAlO_3$; n is the number of EPR line positions fitted simultaneously; $SMD(GHz^2) \equiv \sum_i(\Delta E_i - \nu_i)^2$, where ΔE_i is the calculated energy difference (in GHz) between the levels participating in resonance for the i^{th} line position; ν_i is the corresponding klystron frequency in GHz; h is Planck's constant; and $RMSL(GHz) = (SMD/n)^{1/2}$ is the average room mean-square deviation of energy level difference from klystron frequency. The parameters b_n^m are in GHz. (For conversion to cm^{-1}, use 1 GHz = 0.033565 cm^{-1}).

T (K)	g_z	g_x	g_y	g_{xz}	b_2^0	b_2^2	b_4^0
295	1.989 ±0.001	1.999 ±0.001	1.995 ±0.001	0.00 ±0.01	-1.922 ±0.003	+0.046 ±0.003	-0.015 ±0.001
77	1.985 ±0.006	1.992 ±0.006	1.992 ±0.001	0.00 ±0.01	-1.923 ±0.006	+0.058 ±0.006	+0.002 ±0.006

T (K)	b_4^2	b_4^4	b_2^1	b_4^1	b_4^3	n	RMSL
295	-0.097 ±0.001	-0.021 ±0.003	+0.08 ±0.001	-0.021 ±0.005	+0.143 ±0.005	323	0.1
77	-0.081 ±0.001	-0.011 ±0.001	+0.11 ±0.001	-0.040 ±0.001	+0.042 ±0.001	142	0.1

Table 2. The calculated using Eq. (3), and experimental Gd^{3+} linewidth (ΔB) ratios, calculated by subtracting the temperature independent part for the various allowed ($M \leftrightarrow M-1$) transitions in $EuAlO_3$ at 295 K, for **B** || X-axis.

Ratios of linewidth	Theoretical	Experimental
$\Delta B(+\frac{1}{2} \leftrightarrow -\frac{1}{2})/\Delta B(\pm\frac{7}{2} \leftrightarrow \pm\frac{5}{2})$	2.38	2.0 ± 0.1
$\Delta B(\pm\frac{3}{2} \leftrightarrow \pm\frac{1}{2})/\Delta B(\pm\frac{7}{2} \leftrightarrow \pm\frac{5}{2})$	2.23	1.8 ± 0.1
$\Delta B(\pm\frac{5}{2} \leftrightarrow \pm\frac{3}{2})/\Delta B(\pm\frac{7}{2} \leftrightarrow \pm\frac{5}{2})$	1.77	1.4 ± 0.1

Figure captions

Figure 1. X-band (9.22 GHz) EPR spectrum of the Gd^{3+} ion in an $EuAlO_3$ single crystal at 295 K (a) and 77 K (b) for the orientation of the external magnetic field, **B,** along the magnetic Z-axis. The Gd^{3+} EPR spectrum at 77 K for B || Y, Y′ axes, shown in (c), reveals that the resonance lines of the two magnetically inequivalent Gd^{3+} ions for the corresponding transitions are coincident; (d) Q-band EPR spectrum of Gd^{3+} in $EuAlO_3$ at 140 K for B | | Z-axis.

Figure 2. X-band (9.22 GHz) angular variation of Gd^{3+} EPR line positions in a $EuAlO_3$ single crystal at 295 K for the orientation of the external magnetic field **B** in the magnetic ZX plane. The experimentally observed variation of EPR lines due to Gd^{3+} ions substituting for Eu^{3+} ions is shown by solid circles, whereas the calculated angular variation is shown by continuous lines and small points. The experimental points not connected by continuous lines are most likely due to ions other than Gd^{3+}.

Figure 3. Energy levels of the Gd^{3+} ion in $EuAlO_3$ for the orientation of **B** || Z-axis; (a) represents the allowed transitions at X-band whereas (b) represents those at Q-band.

.

Figure 4. A plot showing the temperature dependence of the Gd^{3+} EPR linewidth for the transition $1/2 \leftrightarrow 3/2$ for B | | X-axis. The experimental data are shown by solid circles and the points calculated, using Eq. 6, are shown by continuous lines.

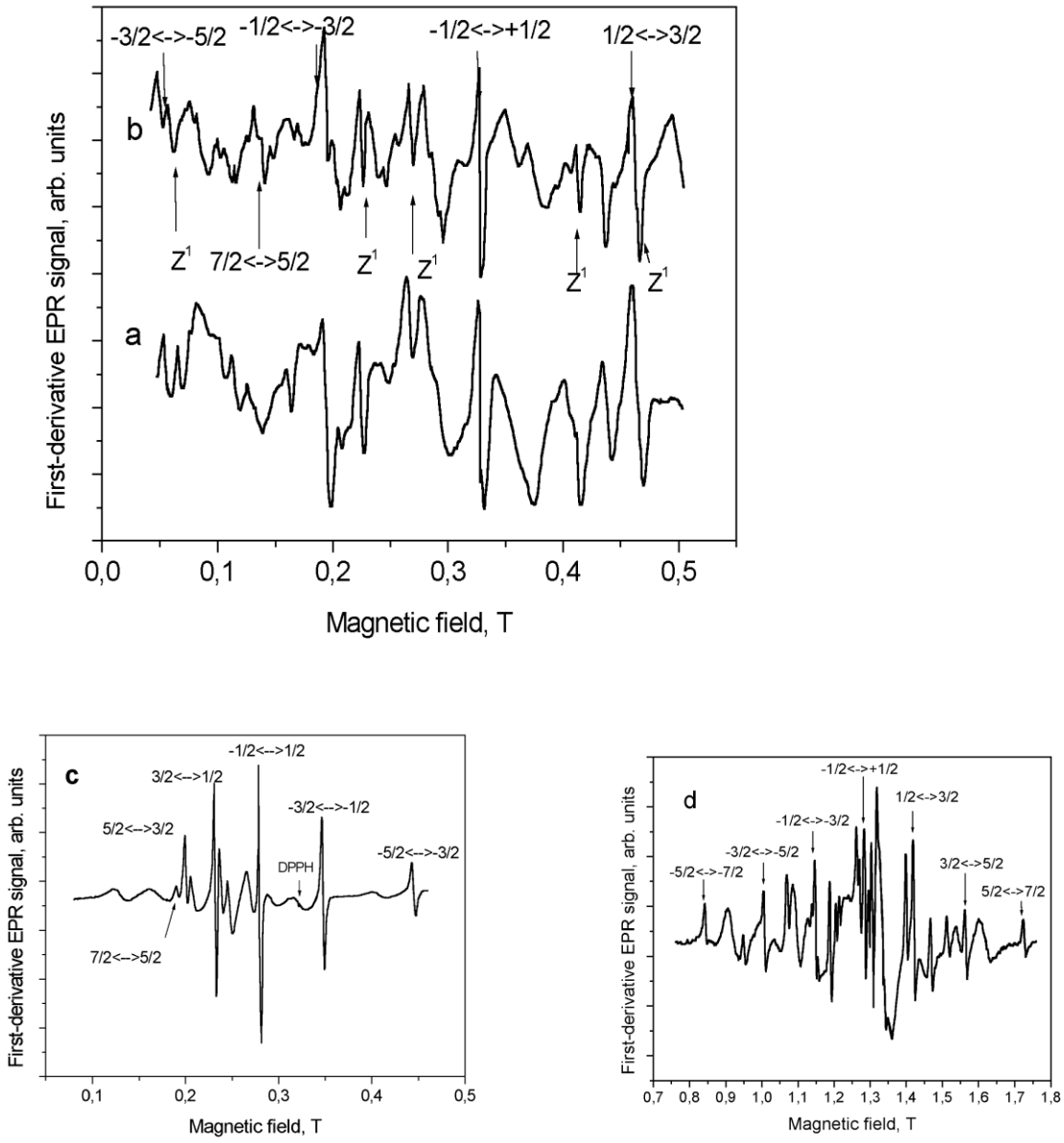

Figure 1. X-band (9.22 GHz) EPR spectrum of the Gd^{3+} ion in an $EuAlO_3$ single crystal at 295 K (a) and 77 K (b) for the orientation of the external magnetic field along the magnetic Z-axis. The Gd^{3+} EPR spectrum at 77 K for B || Y, Y′ axes, shown in (c), reveals that the resonance lines of the two magnetically inequivalent Gd^{3+} ions for the corresponding transitions are coincident; (d) shows Q-band EPR spectrum of Gd^{3+} in $EuAlO_3$ at 140 K and B | | Z-axis.

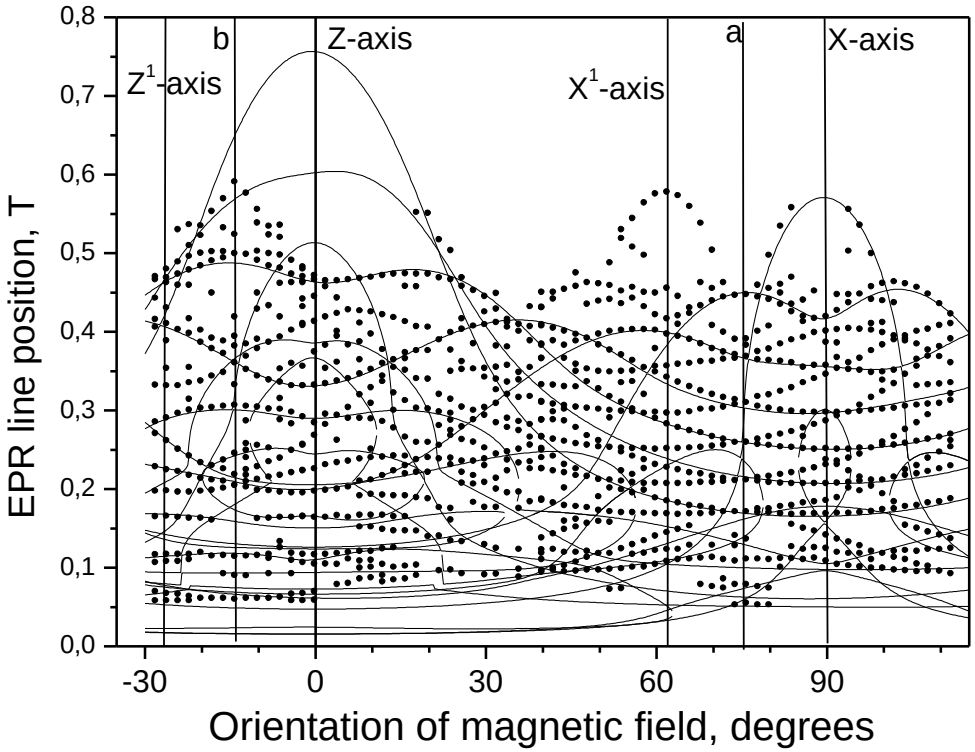

Figure 2. X-band (9.22 GHz) angular variation of Gd^{3+} EPR line positions in a $EuAlO_3$ single crystal at 295 K for the orientation of the external magnetic field in the magnetic ZX plane. The experimentally observed variation of EPR lines due to Gd^{3+} ions substituting for Eu^{3+} ions is shown by solid circles, whereas the calculated angular variation is shown by continuous lines and small points. The experimental points not connected by continuous lines are most likely due to ions other than Gd^{3+}.

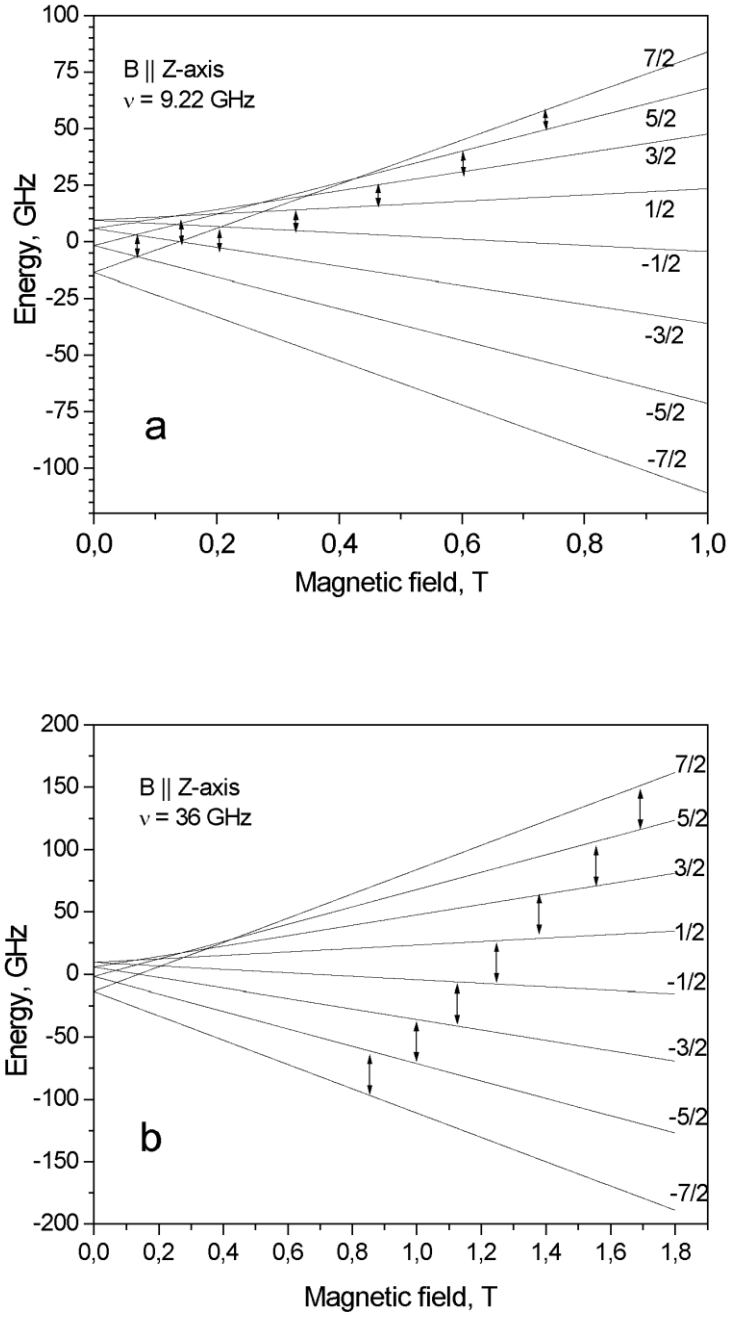

Figure 3. Energy levels of the Gd^{3+} ion in $EuAlO_3$ for the orientation of **B** || Z-axis, (a) represents allowed transitions for X-band and (b) represents that for Q-band.

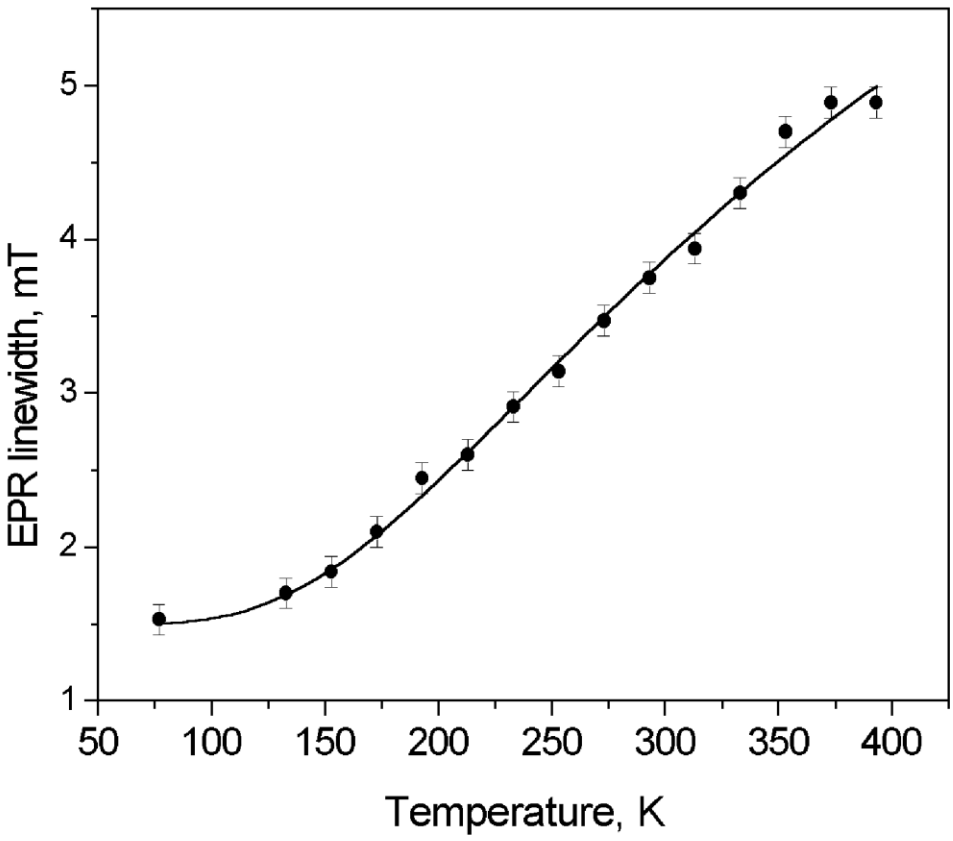

Figure 4. Temperature dependence of the Gd^{3+} EPR linewidth, for the transition $1/2 \leftrightarrow 3/2$ for B | | X-axis. The experimental data are shown by solid circles and the calculated data, using Eq. 6, are shown by continuous line.